



OPEN ACCESS

EDITED BY

Bowen Wu,
Zhejiang University, China

REVIEWED BY

Xueping Li,
Stanford University, United States
Muhammad Shahnawaz Soyfoo,
Université libre de Bruxelles, Belgium

*CORRESPONDENCE

Naiyan Zeng
✉ zengny@shsmu.edu.cn
Xiaochun Fei
✉ xcf0222@163.com
Ning Li
✉ liningman@126.com
Liting Jiang
✉ drjiangliting@163.com

[†]These authors have contributed equally to this work and share the first authorship

RECEIVED 01 February 2023

ACCEPTED 26 June 2023

PUBLISHED 11 July 2023

CITATION

Luo D, Li L, Wu Y, Yang Y, Ye Y, Hu J, Gao Y, Zeng N, Fei X, Li N and Jiang L (2023) Mitochondria-related genes and metabolic profiles of innate and adaptive immune cells in primary Sjögren's syndrome. *Front. Immunol.* 14:1156774. doi: 10.3389/fimmu.2023.1156774

COPYRIGHT

© 2023 Luo, Li, Wu, Yang, Ye, Hu, Gao, Zeng, Fei, Li and Jiang. This is an open-access article distributed under the terms of the [Creative Commons Attribution License \(CC BY\)](https://creativecommons.org/licenses/by/4.0/). The use, distribution or reproduction in other forums is permitted, provided the original author(s) and the copyright owner(s) are credited and that the original publication in this journal is cited, in accordance with accepted academic practice. No use, distribution or reproduction is permitted which does not comply with these terms.

Mitochondria-related genes and metabolic profiles of innate and adaptive immune cells in primary Sjögren's syndrome

Danyang Luo^{1†}, Lei Li^{2†}, Yicheng Wu^{3†}, Yi Yang^{1†}, Yulin Ye¹, Jiawei Hu¹, Yiming Gao¹, Naiyan Zeng^{4*}, Xiaochun Fei^{2*}, Ning Li^{1*} and Liting Jiang^{1*}

¹Department of Stomatology, Ruijin Hospital, Shanghai Jiao Tong University School of Medicine, College of Stomatology, Shanghai Jiao Tong University, Shanghai, China, ²Department of Pathology, Ruijin Hospital, Shanghai Jiao Tong University School of Medicine, Shanghai, China, ³Core Facility of Basic Medical Sciences, Shanghai Jiao Tong University School of Medicine, Shanghai, China, ⁴Key Laboratory of Cell Differentiation and Apoptosis of Chinese Ministry of Education, Department of Pathophysiology, Shanghai Jiao Tong University School of Medicine, Shanghai, China

Background: Primary Sjögren's syndrome (pSS) is a prototypical systemic autoimmune disease characterised by lymphocyte infiltration and immune-complex deposition in multiple organs. The specific distribution of immune cell populations and their relationship with mitochondria remain unknown.

Methods: Histological analysis was performed to assess the specific distribution of innate and adaptive immune cell populations in labial salivary gland (LSG) samples from 30 patients with pSS and 13 patients with non-pSS. The ultrastructural morphometric features of mitochondria within immune cells were observed under the transmission electron microscope (TEM). RNA sequencing was performed on LSG samples from 40 patients with pSS and 7 non-pSS patients. The Single-sample Gene Set Enrichment Analysis (ssGSEA), ESTIMATE, and CIBERSORT algorithms and Pearson correlation coefficients were used to examine the relationship between mitochondria-related genes and immune infiltration. Weighted Gene Co-expression Network Analysis (WGCNA) was used to identify the mitochondria-specific genes and the related pathways based on the immune cell types.

Results: HE staining revealed a massive infiltration of plasma cells with abundant immunoglobulin protein distributed around phenotypically normal-appearing acinar and ductal tissues of patients with pSS. Immunohistochemical analyses revealed that innate immune cells (macrophages, eosinophils and NK cells) were distributed throughout the glandular tissue. Dominant adaptive immune cell infiltration composed of B cells, CD4⁺ T cells and CD8⁺ T cells or ectopic lymphoid follicle-like structures were observed in the LSGs of patients with pSS. TEM validated the swelling of mitochondria with disorganised cristae in some lymphocytes that had invaded the glandular tissue. Subsequently, bioinformatic analysis revealed that innate and adaptive immune cells were associated with different mitochondrial metabolism pathways. Mitochondrial electron transport and respiratory chain complexes in the glandular microenvironment were positively correlated with innate immune cells, whereas amino acid and

nucleic acid metabolism were negatively correlated with adaptive immune cells. In addition, mitochondrial biogenesis and mitochondrial apoptosis in the glandular microenvironment were closely associated with adaptive immune cells.

Conclusion: Innate and adaptive immune cells have distinct distribution profiles in the salivary gland tissues of patients with pSS and are associated with different mitochondrial metabolic pathways, which may contribute to disease progression.

KEYWORDS

Sjogren's syndrome, mitochondria, mitochondrial metabolism, immune cell, transcriptomics, RNA sequencing

Introduction

Primary Sjögren syndrome (pSS) is a systemic autoimmune disease characterised by dryness in the mouth and eyes, chronic pain and fatigue and several other extraglandular manifestations (1). The underlying pathological mechanism is complex and remains unclear. The histopathological features of pSS primarily manifest as lymphocytic infiltration and immune-complex deposition (2). Labial salivary gland (LSG) biopsy is usually used in the diagnosis of pSS, in which the focus score (FS) of ≥ 1 (i.e. ≥ 1 focus per 4 mm²) indicates a positive result (3, 4). The most characteristic feature of pSS is focal lymphocytic sialadenitis (FLS), which is used in the classification of pSS (3). FLS is characterised by infiltration of T and B lymphocytes. B cell activation-mediated clinical manifestations in the pathogenesis of pSS may increase the risk of B-cell lymphoma (5). Accumulation of B and T cells occurs in the advanced and early stages of pSS, respectively. Cytotoxic T cells are directly involved in the destruction of the LSG (6). Although activated CD4⁺T cells with T helper 1 (Th1) and Th2 phenotypes are present, Th17 and follicular helper T (Tfh) cells predominate and may provide a stimulus for B lymphocytes. In addition to the involvement of type I and type II interferons (IFNs) in the innate immune system, crosstalk exists between IL21 (mainly secreted by Tfh cells) and B cell activating factor (BAFF) during B-cell activation (7).

Individual genetic susceptibility that is affected by multiple environmental factors can influence the development of pSS. Some autoantigens that are expressed by the epithelium of the exocrine glands, such as Ro/SSA and La/SSB, can induce a chronic inflammatory microenvironment that drives and activates the differentiation of immune cells (8). In the local inflammatory microenvironment of exocrine glands, activated immune cells further activate epithelial cells and recruit other immune cells, resulting in the continuous interaction between epithelial and immune cells (1, 8, 9). In response to viral infections, type I IFNs are produced by innate immune cells, including dendritic cells (DCs), to activate T and B cells that produce cytokines and autoantibodies to stimulate DCs to present more autoantigens in

systemic autoimmune diseases (10). However, at present, the exact molecular mechanisms underlying the development of pSS remain unknown.

Mitochondria present in almost all cells are biosynthetic and signalling organelles that support cellular function. They are the metabolic hubs of the cell, regulating energy production by coordinating the electron transport chain (ETC) and tricarboxylic acid (TCA) cycle (11). Recent studies have indicated that mitochondria are necessary for the activation, proliferation and function of immune cells (12, 13), such as monocytes/macrophages (14), T/B cells (12, 15), and DCs (16). Alissafi et al. revealed that regulatory T cells (Tregs) undergo metabolic reprogramming with elevated mitochondrial oxidative stress and a robust DNA damage response during autoimmunity (17). Similarly, the mitochondrial respiratory chain is required for the Tregs suppression capacity (18). The metabolic functions of immune cells heavily rely on mitochondria. Abnormal mitochondrial metabolism of immune cells has been reported in autoimmune diseases, such as rheumatoid arthritis (RA) (19) and systemic lupus erythematosus (SLE) (20). Dysfunctional mitochondria released as components can act as pathogen-associated molecular patterns (PAMPs) and damage-associated molecular patterns (DAMPs), such as mtDNA and reactive oxygen species (ROS), to induce an inflammatory response—mainly in the innate immune system—by activating pattern recognition receptors (PRRs) in pSS (21, 22). In a previous study, we demonstrated the mitochondria-related phenotypic changes in the LSGs of patients with pSS (23). However, the role of mitochondrial dysfunction in immune cells in the pathogenesis of pSS remains unclear. Therefore, understanding the mechanisms underlying immune cell disorders is necessary.

This study aimed to examine the distribution of innate and adaptive immune cells, expression of mitochondrial functional proteins and ultrastructural changes in the mitochondria of immune cells in the LSGs of patients with pSS. Transcriptomic analysis revealed the possible mitochondria-related pathways associated with different immune cells. Additionally, changes in oxidative phosphorylation and the metabolic reprogramming of

mitochondria in innate and adaptive immune cells were observed. Altogether, the findings of this study suggest a relationship between LSG and mitochondrial changes in immune cells, thus laying a foundation for further research into the mechanisms underlying the development of pSS.

Materials and methods

Patients and labial salivary gland biopsy

A total of 90 participants (70 patients with pSS and 20 age- and sex-matched non-pSS sicca controls) were included in this study. pSS was diagnosed according to the 2016 American College of Rheumatology/European League Against Rheumatism (ACR/EULAR) classification criteria (24). Individuals who presented with xerostomia or xerophthalmia but did not meet the ACR/EULAR classification criteria for pSS were classified as non-pSS. LSG samples and clinical information were collected after the patients had signed an informed consent form. No participant was receiving any immunosuppressive or steroid medication at the time of LSG biopsy. This study was reviewed and approved by the Ethics Committee of Ruijin Hospital, Shanghai Jiao Tong University School of Medicine and the Chinese Clinical Trial Registry (ChiCTR2000039820).

Histological staining

The LSG samples were fixed in fresh 4% neutral formaldehyde overnight, placed into an automatic tissue dehydrator for dehydration, embedded in paraffin, and cut into 5-mm-thick serial sections for haematoxylin and eosin (HE) and immunohistochemical (IHC) staining. HE and IHC staining were performed according to the manufacturer's instructions. For IHC staining, the LSG tissue sections were deparaffinised, rehydrated in a graded series of ethanol, subjected to antigen retrieval and blocked. Subsequently, the sections were incubated with primary antibodies (detailed information is listed in [Supplementary Table S1](#)) at 25°C for 20 minutes. The sections were washed with PBS; incubated with secondary antibodies; stained with 3,3'-diaminobenzidine (DAB, K5007, DAKO, Denmark) counterstained with haematoxylin. Thereafter, the sections were visualised using the BOND Polymer Refine Detection kit (DS9800, Leica Biosystems). The experiment was performed on a Leica Bond RX automated staining platform (Leica Biosystems).

Transmission electron microscopy

The ultrastructure of LSGs was visualised *via* transmission electron microscopy (TEM) as described previously (23, 25). LSG tissue samples were fixed in 2.5% glutaraldehyde with 0.1-M phosphate-buffered saline (PBS, pH = 7.4), postfixed in 1% osmium tetroxide and dehydrated in a graded series of ethanol. The samples were embedded in a solution of 812 resin (EMS, TED

PELLA, USA) and propylene oxide and incubated for 48 hours. The samples were transversely cut into sections of 70–90 nm using a diamond knife (EM UC7; Leica, Wetzlar, Germany) and stained with lead citrate. Images were obtained on a transmission electron microscope (H-7650; Hitachi, Japan).

RNA sequencing and basic analysis

The LSGs samples of 40 patients with pSS and 7 patients with non-pSS were used for RNA-seq. Total RNA was extracted using the TRIzol reagent (Invitrogen, USA), quantified on an Agilent 2100 bioanalyser (Agilent Technologies, CA, USA) and a NanoDrop spectrophotometer (Thermo Fisher Scientific Inc.) and separated on 1% agarose gel. 1 µg of total RNA with RIN of >6.5 was used to create the library. The next-generation sequencing library was designed according to the manufacturer's protocol. The prepared library was multiplexed and uploaded to the Illumina Novaseq system (Illumina, CA, USA). The sequence used a 2x-150-bp paired-end (PE) configuration. The HiSeq Control Software (HCS), OLB and GApipeline-1.6 (Illumina) management software were used for image analysis and identification. To eliminate technical errors, Cutadpt (V1.9.1) was used to process the data in the fastq file to obtain clean, high-quality data.

The limma and DEseq2 Bioconductor packages were used to identify differentially expressed genes (DEGs) based on the RNA-seq data ($|\log_{2}FC| > 0.5$, $p < 0.05$). These DEGs were demonstrated on Venn diagrams and volcano plots. Interactive relationships and protein-protein interaction (PPI) networks of the overlapping DEGs were evaluated using the STRING database (<http://string-db.org>) (26). GO functional annotation and Kyoto Encyclopedia of Genes and Genomes (KEGG) pathway enrichment analyses were performed using the cluster profiler package in R (27). Based on the integrated GO and KEGG data, Metascape was used to identify all ontology terms that were significantly common among genes (28). Proteomaps (www.proteomaps.net) based on RNA transcript data were drawn to visualise three levels of functional categories based on KEGG pathway analysis (www.genome.jp/kegg/) (29).

Analysis of immune cell infiltration and the glandular microenvironment

The cell type of each cluster (43 immune cells and 8 salivary glandular compositions) was identified using the CellMarker database and by aligning marker genes to known signature genes reported in previous studies (30). The Stromal, Immune and ESTIMATE scores of LSG samples were calculated using the ESTIMATE R package (<http://bioinformatics.mdanderson.org/estimate/index.html>).

The single-sample gene set enrichment analysis (ssGSEA) (31) and CIBERSORT (<http://cibersort.stanford.edu>) algorithms were used to estimate the proportion of innate and adaptive immune cell types in the LSGs of patients with pSS. The ComplexHeatmap (version 2.10.0) package in R (32) was used to construct heatmaps and perform cluster analysis. The 'pheatmap' package was used to

examine the correlation (Spearman analysis) between the abundance of immune cells and the expression of hub genes.

Weighted gene co-expression network analysis and gene set enrichment analysis

Weighted gene co-expression network analysis (WGCNA) was performed using the R package WGCNA to identify the module most relevant to immune infiltration (33, 34). Modules with interconnected features were screened based on network analysis, correlation coefficients and hierarchical clustering. To identify mitochondria-related genes highly correlated with innate or adaptive immune cells, the hub mitochondria-related genes were selected by intersecting genes in WGCNA modules and genes identified from the Mitocarta 3.0 database (35). GSEA was performed using the GSEA (version 2.0) software (31, 36). Curated gene sets for GSEA were obtained from <http://software.broadinstitute.org/gsea/index.jsp>. Enrichment was considered significant when the p-value was < 0.05. The correlation between hub immune cells and mitochondrial metabolic pathways was examined using the Mantel test and Pearson correlation coefficients in the pSS group and visualized using the 'ggcor' R package (version 0.9.8.1) (<https://github.com/houyunhuang/ggcor>) based on 'ggplot2' package.

Statistical analysis

Statistical analysis was performed using Student's t-test, one-way ANOVA or Chi-square test in the GraphPad Prism. Quantitative data were expressed as the mean ± standard deviation (SD). A p-value of < 0.05 was considered statistically significant.

Results

Distribution and proportion of innate and adaptive immune cells in the LSGs of patients with pSS

A flowchart illustrating the overall study protocol is shown in Figure 1. A total of 70 patients with pSS and 20 sex- and age-matched Non-pSS patients were included. The clinical data of all participants were collected from their medical records (Table 1). Patients with FS of ≥ 1 and anti-SSA antibody-positive status were included in the pSS group, whereas those with FS of < 1 and anti-SSA antibody-negative status were included in the control group. Patients in the pSS group were found to have elevated serum IgG levels (17.98 ± 7.72 versus 12.94 ± 3.09 g/L, p < 0.01), ANA-positive status (94.3% versus 65%, p < 0.01), anti-Ro52-positive status

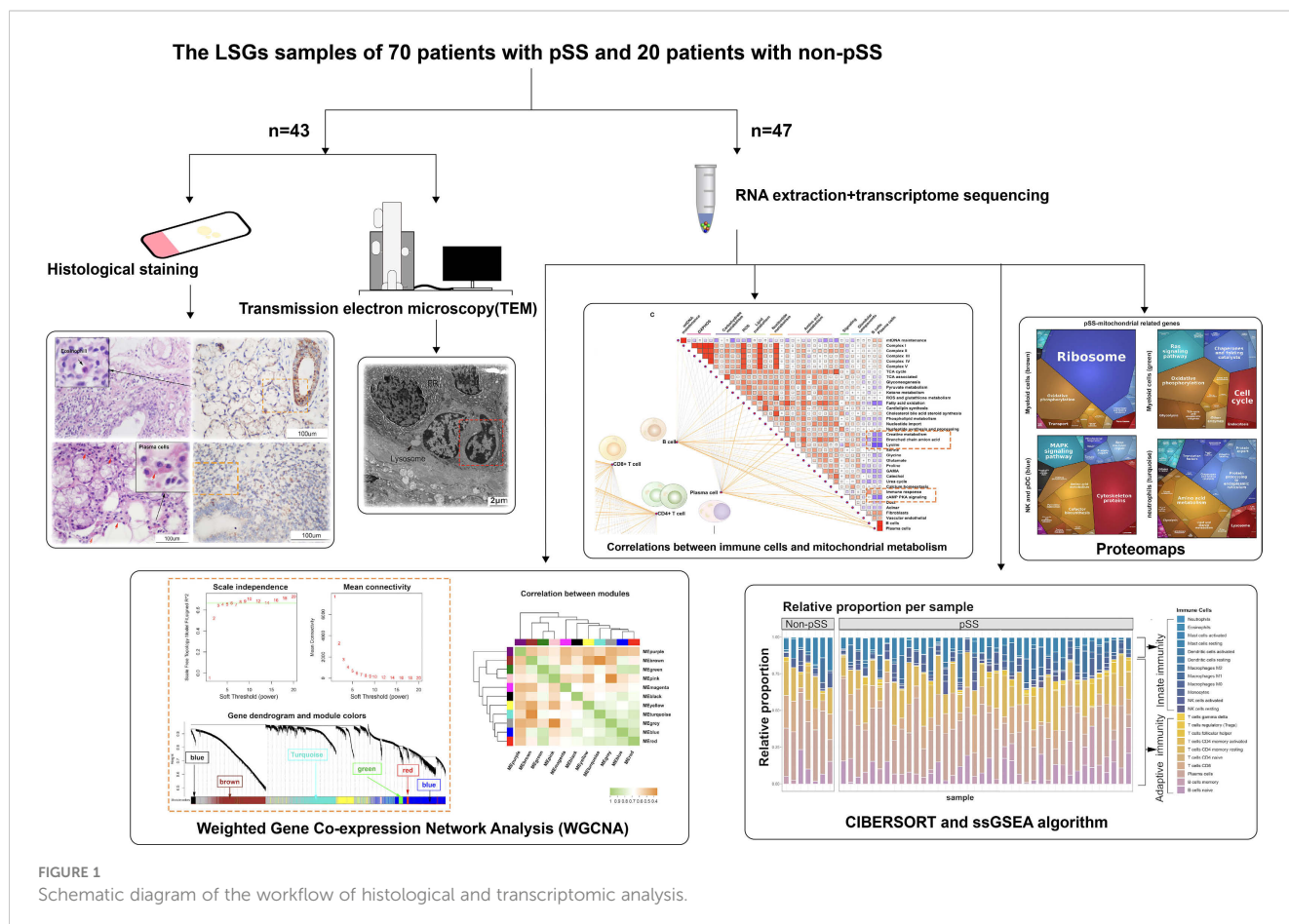


FIGURE 1 Schematic diagram of the workflow of histological and transcriptomic analysis.

TABLE 1 Clinical data of patients with pSS and Non-pSS included in this study.

	pSS (n=70)	Non-pSS (n=20)
Gender (Female)	57/70	18/20
Age	52.04 ± 10.01	52.90 ± 9.14
Chisholm Grade	3: 44	0: 11
	4: 26	1: 4
	–	2: 5
ANA+ (%)	94.3**	65
Anti-SSA+ (%)	100	0
Anti-Ro52+ (%)	77.1**	45
Anti-SSB+ (%)	41.4***	0
IgG (g/L)	17.98 ± 7.72**	12.94 ± 3.09
IgA (g/L)	2.92 ± 1.22	2.43 ± 0.95
IgM (g/L)	1.43 ± 0.90	1.55 ± 0.92
C3 (g/L)	1.05 ± 0.28	1.12 ± 0.21
C4 (g/L)	0.25 ± 0.10	0.29 ± 0.14
Hypocomplementemia	6/70	2/18
ESSDAI	3.87 ± 1.12	0

Data are mean ± standard deviation (SD) or n (%). *p<0.05; **p<0.01; ***p<0.001. ANA, anti-nuclear antibody. ESSDAI, EULAR Sjögren's Syndrome Disease Activity Index.

(77.1% versus 45%, $p < 0.01$), and anti-SSB-positive status (41.4% versus 0, $p < 0.001$).

HE staining was performed to visualise the distribution of immune cells in the LSGs of patients in both groups. In the pSS group, the structure of LSGs was destroyed, and excessive infiltration of immune cells was observed in LSGs (Figure 2A). A large number of plasma cells (red arrow) containing immunoglobulins was distributed around the acini and ducts. Similarly, the deposition of abnormal immunoglobulins was found in morphologically normal acini and ductal tissues. Some regions showed lymphoepithelial lesions (LELs) and germinal centre (GC)-like structures. According to morphological characteristics, a few eosinophils were scattered at the periphery of the lesions. Macrophages were mainly distributed in the residual glandular epithelial/myoepithelial regions. Conventionally, the glandular tissue of non-pSS patients had very small low levels of immune cell infiltration, and fewer plasma cells containing immunoglobulins (Figure 2B).

Salivary gland tissues subjected to RNA sequencing were analysed to quantify immune cell infiltration using CIBERSORT, ESTIMATE, and ssGSEA algorithms. CIBERSORT was used to calculate the proportion of 22 immune cell types, and the results showed that adaptive immune cells primarily infiltrated the LSGs of patients with pSS (Figure 2C). The results of ssGSEA showed that the proportion of infiltrating immune cells (both innate and adaptive) in LSGs was significantly higher in the pSS group than in the control group ($p < 0.05$) (Figure 2D). Furthermore, the relationship between the abundance of immune cells and expression

of genes related to glandular tissue and mitochondria was examined (Figures 2E, F). The abundance of almost all immune cells was negatively correlated with the expression of marker genes of acini (mainly serous acini) and progenitor cells and the mitochondrial biogenesis-related gene PPARGC1A. However, it was positively correlated with the expression of marker genes of vascular endothelial cells and fibroblasts and mitochondria-related genes (BCL2 and COX4L2). The expression of marker genes of ducts and myoepithelial cells (MECs) was negatively correlated with the abundance of B cells and innate immune cells, respectively (Figure 2E). These results were verified in the pSS and control groups. Conventionally, the expression of BCL2 gradually increased and that of PPARGC1A decreased with the increase in FS. The ESTIMATE algorithm was used to assess the overall immune infiltration and stromal content (37). The results revealed that the pSS group had significantly higher Immune, Stromal, and ESTIMATE scores. These results were consistent with those of ssGSEA. In addition, the expression of the mitochondria-related genes cytochrome c oxidase (COX) -IV and cytochrome c (CYCS) was associated with the pathological features of pSS (Figure 2F). Altogether, these results indicate that the specific glandular microenvironment alters the proportion and distribution of immune cells and is associated with mitochondrial function.

Histological analysis of innate immune cell infiltration in the LSGs of patients with pSS

To characterise immune cells in the immune microenvironment of pSS, the cells were divided into innate and adaptive immune cell populations. The infiltration of innate immune cells was validated *via* IHC staining (Figure 3). A panel of innate immune cell-related markers was used, and ssGSEA was used to calculate infiltration scores based on RNA-seq data. Cytokeratin 7 (CK7, K7 or KRT7) is one of the marker genes of the salivary gland epithelium (38). Based on the analysis of CK7 expression, the LSG epithelium was found to be intact in the control group. However, almost no CK7 expression was observed in regions with infiltrated lymphocytes in patients with pSS. CK7 expression in the centre of FLS represented an epithelioid mass in regions with infiltrated lymphocytes. The antiapoptotic B-cell lymphoma 2 (BCL2) family members, including BCL2, can suppress autophagy and cell death and have been associated with ROS adaptation (39). BCL2 expression was high in not only acini and ducts in the non-pSS group but also regions with infiltrated lymphocytes in the pSS group. CD45 is expressed on all nucleated haematopoietic cells that can distinguish immune cells from salivary gland epithelial cells (40). Some epithelial tissue was observed in FLS, which was consistent with the results of CK7 staining analysis. CD21, a marker of follicular dendritic cells (FDCs), represents the GC structure (3). Arginase-1 is a marker of M2 polarisation, whereas CD68 represents the total macrophages (41). CD56 is known as a phenotypical marker of natural killer (NK) cells (42). FDCs, macrophages and NK cells were observed in the LSGs of pSS patients. FDCs were expressed in the GC, whereas macrophages, mainly M2 macrophages, and NK cells were distributed around the infiltrating foci. The expression of the marker genes of innate immune

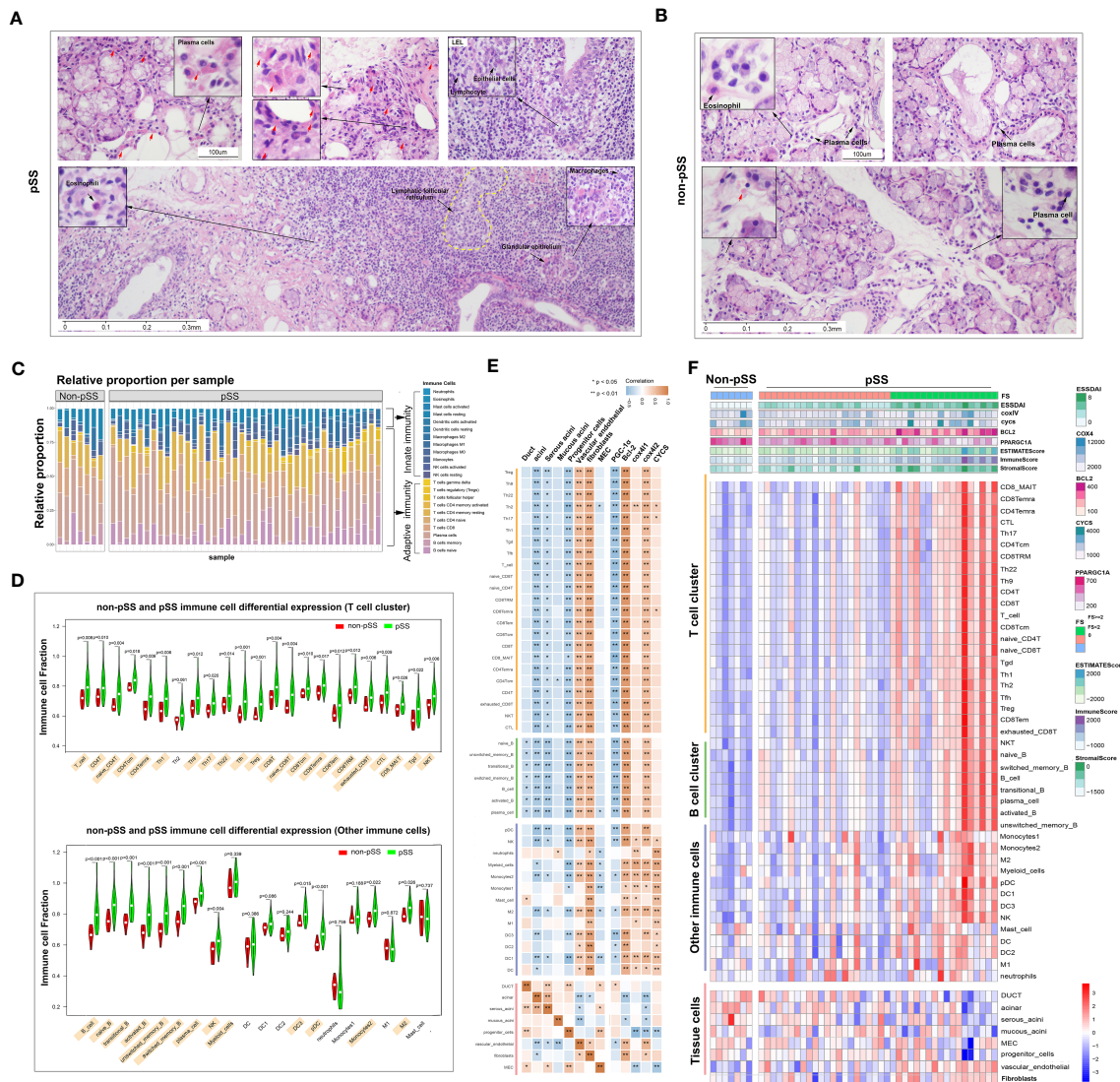


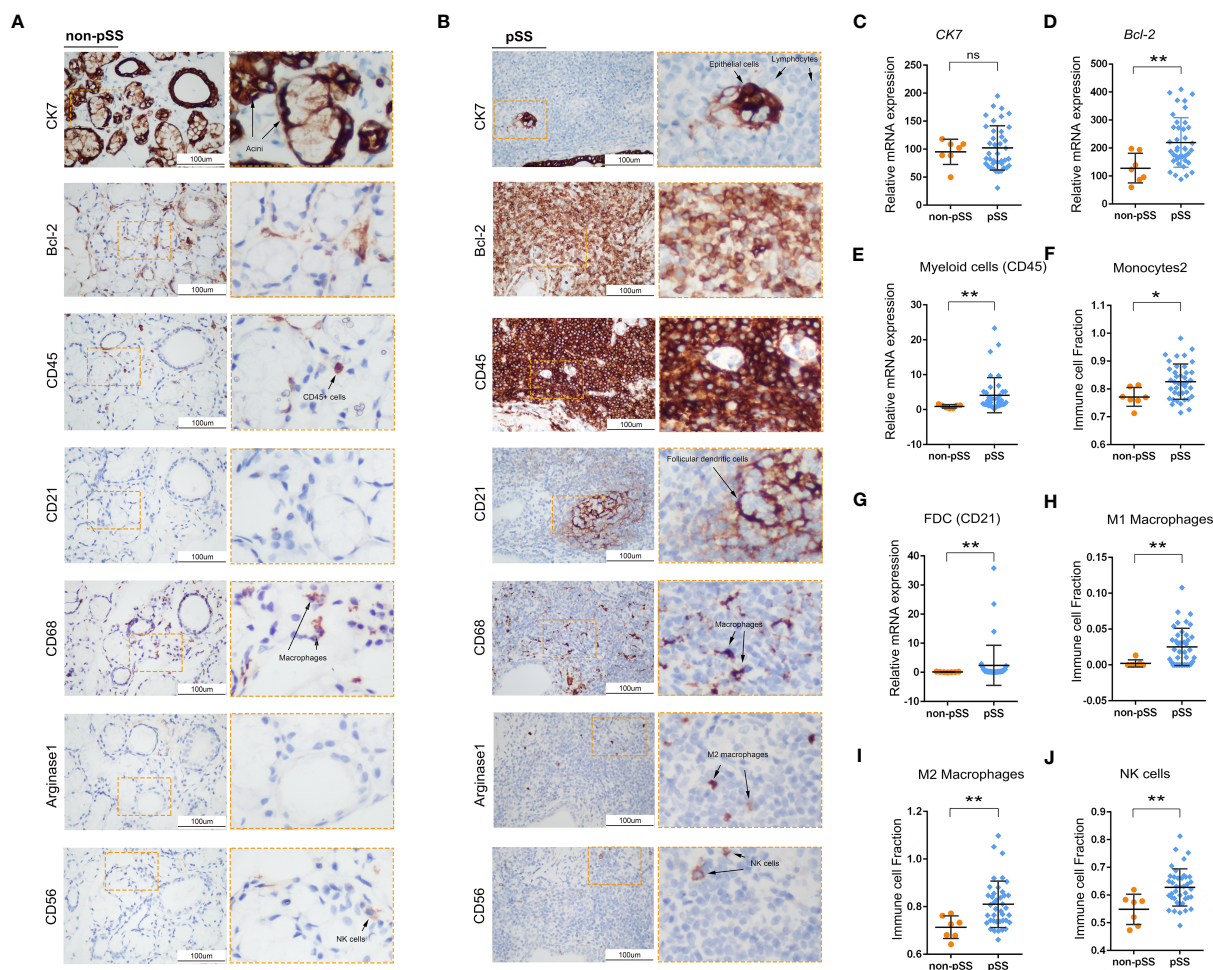
FIGURE 2
 Distribution and proportion of innate and adaptive immune cells in the immune microenvironment of labial salivary glands (LSGs) of patients with primary Sjogren's syndrome (pSS). **(A)** Histological features of focal lymphocytic sialadenitis (FLS) in the LSGs of patients with pSS, including lymphoepithelial lesions (LELs) and germinal centre (GC)-like structures. The red arrow represents plasma cells containing immunoglobulins (haematoxylin and eosin staining; original magnification at $\times 100$ or $\times 400$). **(B)** Various immune cells were scattered in the glandular tissue of patients without pSS (haematoxylin and eosin staining; original magnification at $\times 200$ or $\times 400$). **(C)** The proportion of innate and adaptive immune cells infiltrating the glandular tissue was determined using the CIBERSORT algorithm. **(D)** Violin plot demonstrating the abundance of 43 types of immune cells evaluated using the ssGSEA algorithm. **(E)** Correlation between the expression of marker genes of the salivary gland and mitochondria and the abundance of immune cells in LSGs in the pSS and control groups. Orange represents a positive correlation, and blue represents a negative correlation. **(F)** Heatmap demonstrating the enrichment scores of the abovementioned genes and immune cells evaluated using the ssGSEA algorithm and stromal, immune and ESTIMATE scores calculated using the ESTIMATE algorithm. Each column represents an individual patient sample, and each row represents an individual gene or immune cell type, ordered *via* unsupervised hierarchical clustering.

cells all showed an upward trend in the pSS group based on the RNA-seq (Figure S1). The results of histological analysis were consistent with those of RNA-seq, suggesting that the RNA-seq data were reliable.

Expression patterns of mitochondria-related genes in innate immune cells

The ssGSEA scores of 12 innate immune cell types were used as phenotypic data for the WGCNA analysis to identify co-expressed

genes and examine the correlation between gene modules and phenotypes. A total of 11 modules were displayed in different colours (Figure 4A). The correlation between different modules is presented in Figure 4B. Furthermore, the correlation between genes in these modules and marker genes of innate immune cells was examined (Figure 4C). The expression of genes in four modules, including brown, green, black and blue modules, was significantly positively correlated with the abundance of almost all types of innate immune cells. The turquoise module contained most genes, and the expression of these genes was significantly negatively



correlated with only three cell types, including myeloid cells, neutrophils, and type 2 monocytes.

Metascape was used to identify signalling pathways associated with genes in the brown and blue modules. Based on the integrated results of GO and KEGG analyses, metabolic processes were mainly associated with genes in the brown module (Figure 4D). However, leukocyte activation, regulation of activation and positive regulation of immune response were associated with genes in the blue module (Figure 4E). Subsequently, the genes of the two modules were merged and intersected with mitochondria-related genes to obtain 561 genes as shown in the Venn diagram in Figure 4F. Based on these 561 genes, a hub term enrichment network was constructed using Metascape. Respiratory chain-related signalling pathways were at the core of the enrichment network. Furthermore, we selected four modules with a significant correlation and intersected genes in these modules with mitochondria-related genes. KEGG analysis of the overlapping genes revealed that pathways associated with ribosomes and

oxidative phosphorylation were dominant in the brown module corresponding to myeloid cells (Figure 4G). Similarly, pathways associated with oxidative phosphorylation and Ras signalling were dominant in the green module corresponding to myeloid cells, those associated with cytoskeleton proteins and MAPK signalling were dominant in the blue module corresponding to NK cells and pDCs and those associated with amino acid, lipid and steroid metabolism were dominant in the turquoise module corresponding to neutrophils.

Owing to the high enrichment of metabolic processes (Figure 4D), we investigated the potential correlation among innate immune cells, glandular tissue and mitochondrial metabolism in the pSS group. The Mantel test was used for statistical analysis, and pattern diagrams were drawn (Figure 5). The abundance of innate immune cells (DC1, NK cells, myeloid cells, type 1 and 2 monocytes and M1 and M2 macrophages) was strongly positively correlated with the mitochondrial respiratory chain complex, fibroblast abundance, immune response, lipid

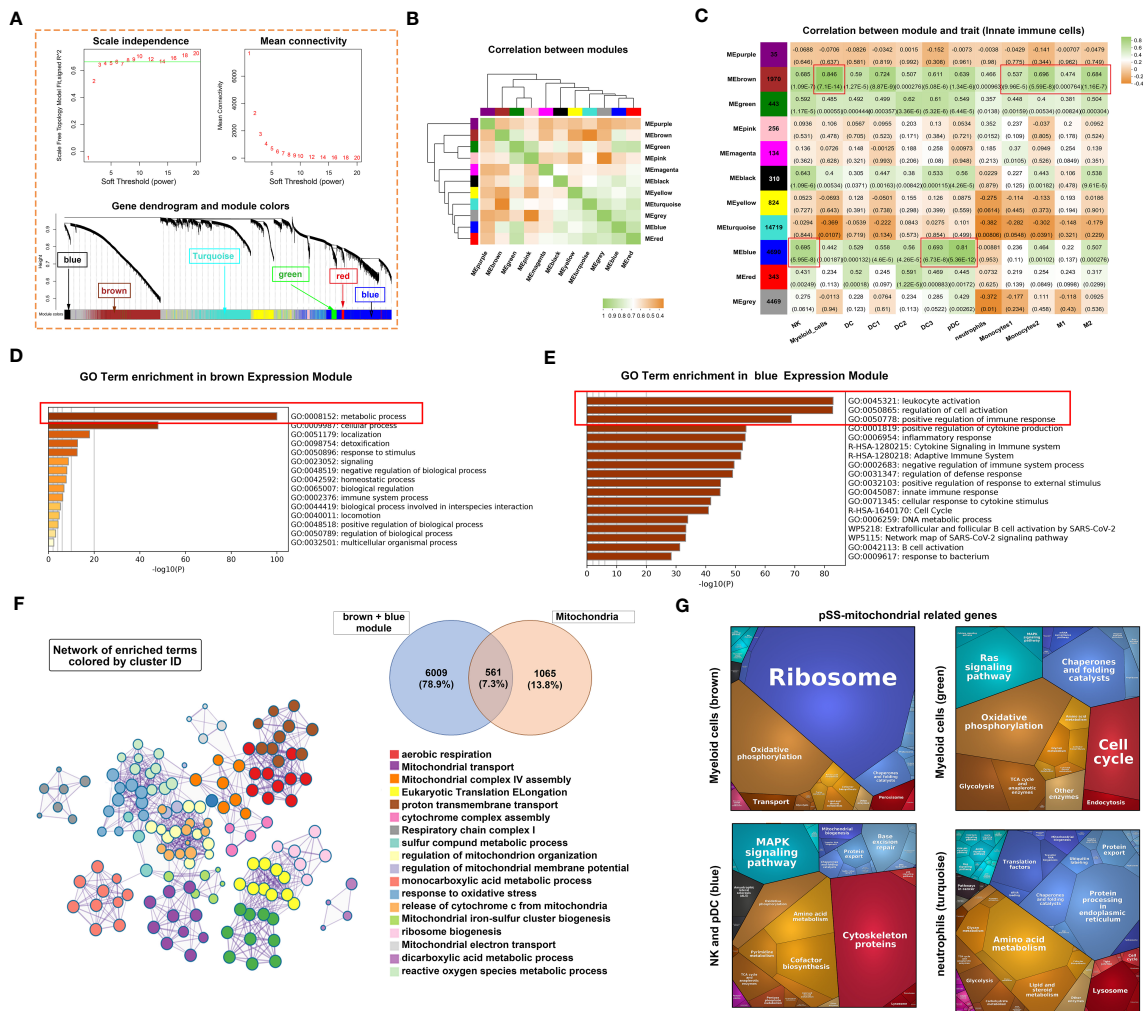


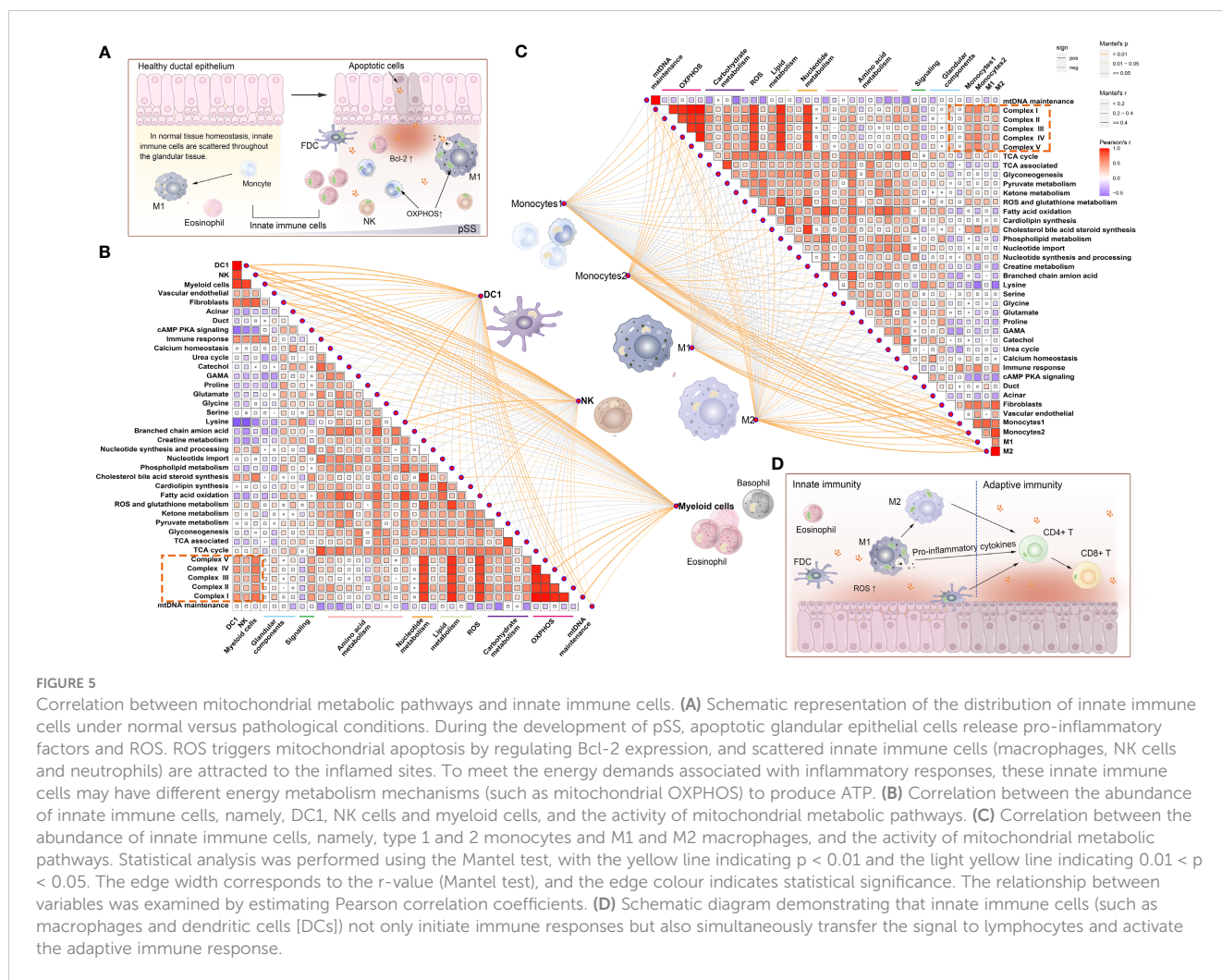
FIGURE 4 Innate immune-related co-expression network generated using WGCNA and mitochondrial-related gene enrichment analysis. **(A)** Analysis of the scale-free fit index (upper left panel) and the mean connectivity for various soft-thresholding powers (upper right panel). Different colours represent different gene modules (lower panel). **(B)** Hierarchical clustering correlation among WGCNA modules. A total of 11 gene co-expression modules were identified. **(C)** Heatmap demonstrating module–trait relationships. Green indicates a positive correlation and orange indicates a negative correlation between the expression of genes in the modules and the abundance of innate immune cells. The number in each immune cell indicates the correlation coefficient and p-value. **(D, E)** Bar graph demonstrating the results of GO functional annotation analysis performed using Metascape in the brown **(D)** and blue **(E)** modules. **(F)** Significantly enriched clusters marked in different colours in the network were annotated using Metascape (left panel). Different colours represent different GO terms. The Venn diagram (right panel) demonstrates the 561 overlapping genes between mitochondria-related genes and genes in the brown and blue modules. **(G)** Heatmap demonstrating functional categories in three innate immune cell types (different modules) as identified using Proteomaps (www.proteomaps.net). Each protein encoded by a known ID gene is represented by a polygon, and functionally related proteins are arranged in common and similar regions.

metabolism and nucleotide synthesis. However, it was significantly negatively correlated with acinar cell abundance, cAMP–PKA signalling and amino acid metabolism (Figures 5B, C). Altogether, these results suggest that mitochondria-related metabolic pathways in innate immune cell populations are altered in patients with pSS.

Adaptive immune cells were mainly distributed in the central region of the FLS in the LSGs of patients with pSS

The distribution of adaptive immune cells was assessed *via* IHC staining. The expression of COX-IV, a subunit of COX translocation

proteins, was high not only in ductal epithelial cells in the control group but also in the immune cells of lymphoid infiltrating lesions in the pSS group (Figure 6B). Matrix metalloproteinase 9 (MMP9) is a family of endopeptidases that regulate extracellular matrix remodelling and contribute to the development of fibrosis (43). In the LSGs of patients with pSS, MMPs were expressed in clumps in the centre of lesions (Figure 6D). Additionally, CD3 (T cells), CD4 (T cells) and CD20 (B cells) were mainly expressed in the centre of FLS and constituted the main part of the GC structure (Figures 6F, J, N). CD8 (T cells), Foxp3 (Tregs) and CD38 (plasma cells) were scattered in the periphery of GC (Figures 6H, L, P). The expression of marker genes in adaptive immune cells is shown in Figure S2. The expression of CD3D (T cells) and MS4A1 (B cells) was low in the control group,



whereas the distribution of CD38 (plasma cell) was consistent with the results of HE staining (Figures 6O, P, 2B). These cell distribution trends were consistent with those observed in RNA-seq analysis and ssGSEA scores (Figures 6A, C, E, G, I, K, M, S2).

As mitochondrial function is closely associated with mitochondrial morphology, dysfunctional mitochondria are swollen and fragmented, whereas healthy mitochondria are thin and long. TEM was used to observe the ultrastructure of mitochondria in the immune cells of LSGs. As shown in Figure 7A, lymphocyte infiltration was very low in normal glandular tissues and interstitium. Healthy lymphocytes have less cytoplasm, normal mitochondrial morphology and clear mitochondrial cristae. In the pSS group, more lymphocytes were found to invade the basement membrane of the acini, ducts and interstitium. Although the surrounding acinar cells exhibited endoplasmic reticulum stress and karyopyknosis, the invading lymphocytes retained the morphological features of mitochondrial cristae (Figure 7B). However, lymphocytes with swollen mitochondria and broken cristae and lysosomes were seen in the interstitial fibrous tissue (Figures 7B, C). These changes did not occur in all lymphocytes but were only partially visible (Figure 7D). Although ductal cells

contained massively swollen mitochondria, some invading lymphocytes had normal mitochondria.

Patterns of mitochondria-related metabolism in adaptive immune cells were similar to those in innate immune cell

The ssGSEA scores of 22 types of T and B cells and FS were selected as phenotypic data for WGCNA to identify co-expressed genes and examine the inter-relationship among gene modules, pathological features and phenotypes (Figures 8A, B). The expression of genes in the blue and black modules had the strongest correlation with the abundance of adaptive immune cell populations. Genes in these two modules were integrated and intersected with mitochondria-related genes to obtain 207 genes. Metascape was used to construct the corresponding enrichment term networks for these overlapping genes, and the results are shown in the Venn diagram in Figure 8C. The term 'release of cytochrome c from mitochondria' was at the centre of the network (Figure 8C), whereas the term 'mitochondrion organization' had the highest enrichment score (Figure 8D).

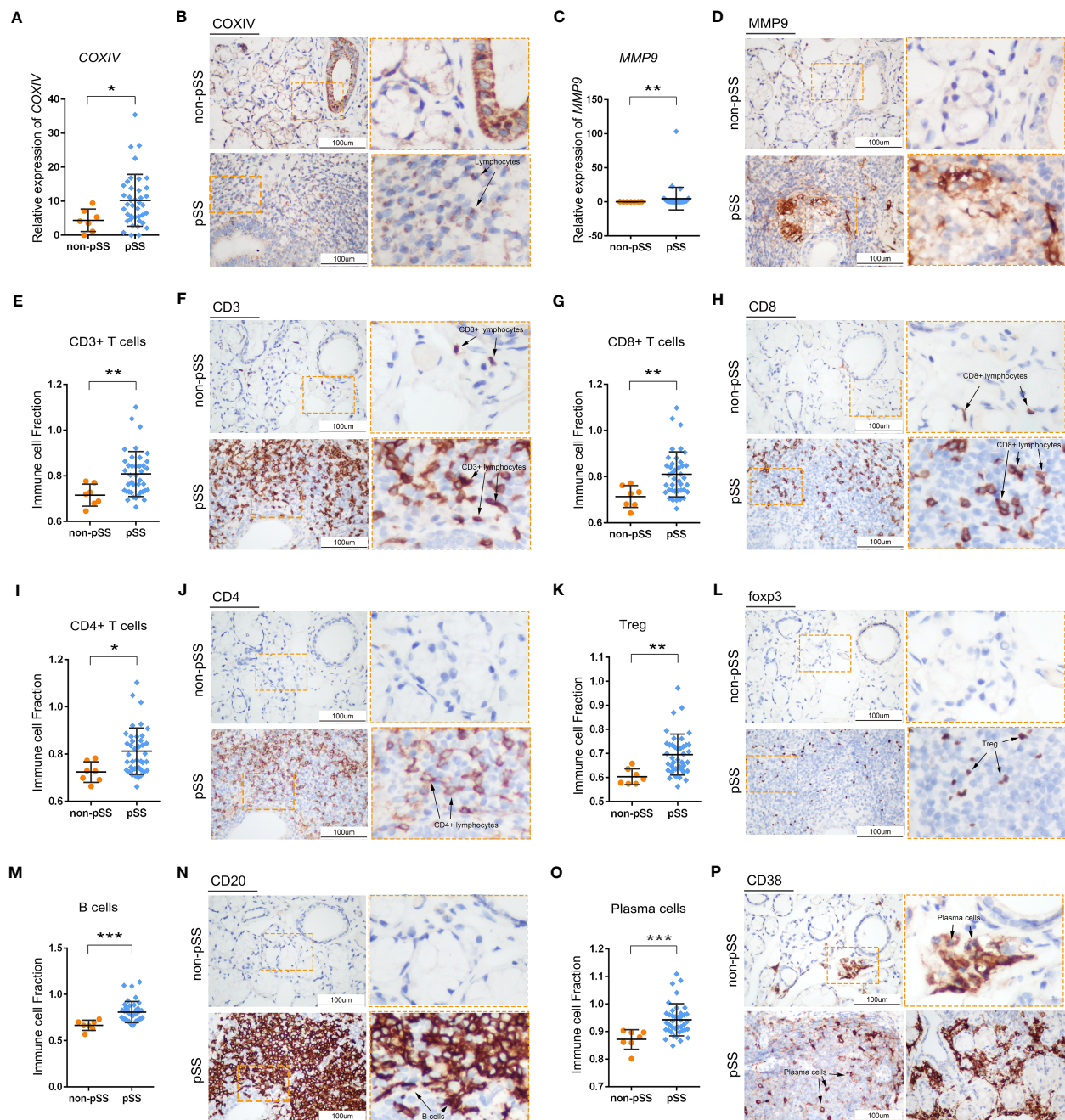


FIGURE 6

Histological analysis of adaptive immune cells in LSG tissues. (A, B) Statistical analysis of COX-IV expression based on RNA-sequencing data (A) and representative images of IHC staining for COX-IV (B) in human LSGs in the control and pSS groups (scale bar = 100 μ m) (*, $p < 0.05$). (C–D) Statistical analysis of MMP9 expression based on RNA-sequencing data (C) and representative images of IHC staining for MMP9 (D) in human LSGs in the control and pSS groups (scale bar = 100 μ m) (**, $p < 0.01$). (E, F) Statistical analysis of CD3 immune infiltration and ssGSEA scores based on RNA-sequencing data (E) and representative images of IHC staining for CD3 (F) in human LSGs in the control and pSS groups (scale bar = 100 μ m) (**, $p < 0.01$). (G, H) Statistical analysis for CD8 immune infiltration and ssGSEA scores based on RNA-sequencing data (G) and representative images of IHC staining for CD8 (H) in human LSGs in the control and pSS groups (scale bar = 100 μ m) (**, $p < 0.01$). (I, J) Statistical analysis of CD4 immune infiltration and ssGSEA scores based on RNA-sequencing data (I) and representative images of IHC staining for CD4 (J) in human LSGs in the control and pSS groups (scale bar = 100 μ m) (*, $p < 0.05$). (K, L) Statistical analysis of Treg infiltration and ssGSEA scores based on RNA-sequencing data (K) and representative images of IHC staining for Foxp3 (L) in human LSGs in the control and pSS groups (scale bar = 100 μ m) (**, $p < 0.01$). (M, N) Statistical analysis of B-cell infiltration and ssGSEA scores based on RNA-sequencing data (M) and representative images of IHC staining for CD20 (N) in human LSGs in the control and pSS groups (scale bar = 100 μ m) (***, $p < 0.001$). (O, P) Statistical analysis of plasma cell infiltration and ssGSEA scores based on RNA-sequencing data (O) and representative images of IHC staining for CD38 (P) in human LSGs in the control and pSS groups (scale bar = 100 μ m) (***, $p < 0.001$).

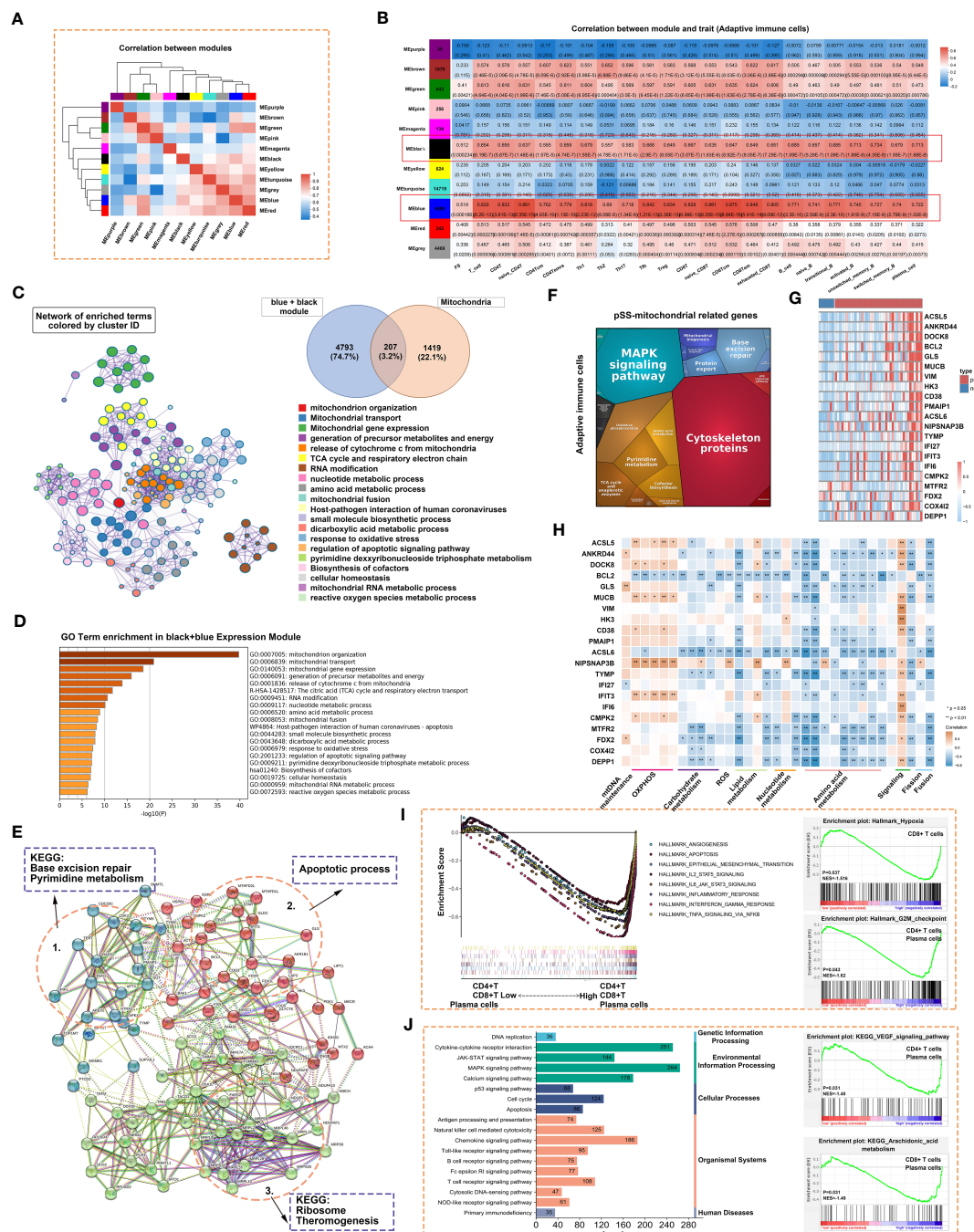
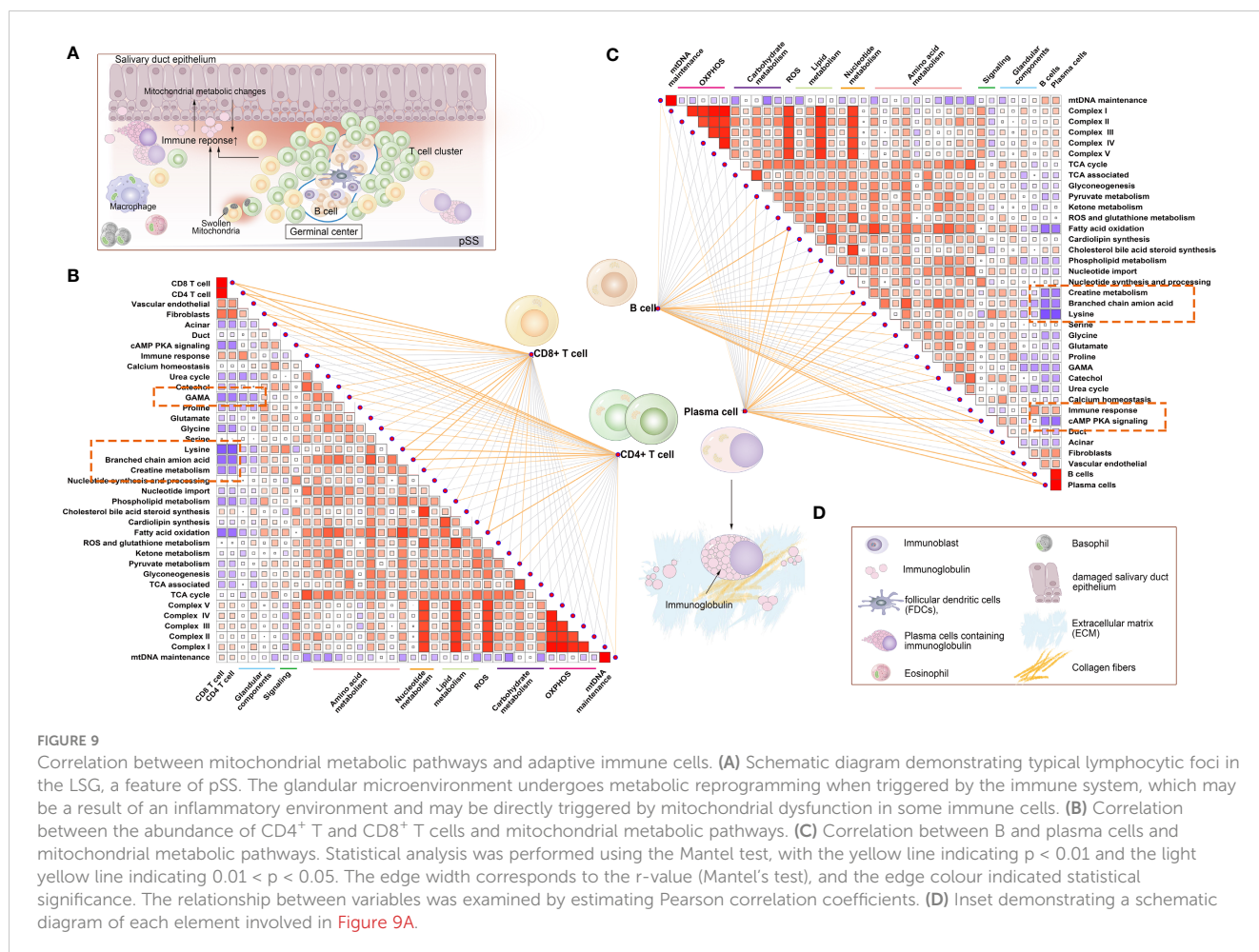


FIGURE 8 Adaptive immune-related co-expression network generated using WGCNA and mitochondrial-related gene enrichment analysis. **(A)** Hierarchical clustering correlation among WGCNA modules. A total of 11 gene co-expression modules were identified. **(B)** Heatmap demonstrating module–trait relationships. Green indicates a positive correlation and orange indicates a negative correlation between the expression of genes in the modules and the abundance of innate immune cells. The number in each immune cell indicates the correlation coefficient and p-value. **(C)** Significantly enriched clusters marked in different colours in the network were annotated using Metascape (left panel). Different colours represent different GO terms. The Venn diagram (right panel) demonstrates the 207 overlapping genes between mitochondria-related genes and genes in the black and blue modules. **(D)** Bar graph demonstrating the results of GO functional annotation analysis of the 207 genes performed using Metascape. **(E)** PPI network revealed three clusters related to pyrimidine metabolism, apoptosis and ribosomes. **(F)** Heatmap demonstrating the functional categories of adaptive immune cells based on the 207 mitochondria-related genes as examined using Proteomaps. Each protein encoded by a known ID gene is represented by a polygon, and functionally related proteins are arranged in common and similar regions. **(G)** Heatmap of 21 differentially expressed genes related to mitochondria. **(H)** The correlation between the 21 genes and mitochondrial metabolic pathways was examined via Pearson correlation analysis. Orange indicates a positive correlation, whereas blue indicates a negative correlation (*, $p < 0.05$; **, $p < 0.01$). **(I)** GSEA was used to evaluate the abundance of CD4⁺ T, CD8⁺ T and plasma cells in the Hallmark gene set. **(J)** GSEA was used to evaluate the abundance of CD4⁺ T, CD8⁺ T and plasmas in the KEGG gene set.



CD4⁺ T and plasma cells and arachidonic acid metabolism was shared by CD8⁺ T and plasma cells in the KEGG gene set (Figure 8J).

The correlation between the abundance of CD4⁺ T, CD8⁺ T, B and plasma cells and the expression of mitochondria-related genes was examined (Figure 9). Similar to innate immune cells, these adaptive immune cells were negatively correlated with mitochondrial metabolism and positively correlated with immune responses and respiratory chain complexes.

Discussion

This study demonstrated the infiltration characteristics of innate and adaptive immune cells in the LSGs of patients with pSS and the ultrastructure of mitochondria in the two types of immune cells. Mitochondria-related metabolic pathways in innate and adaptive immune cells were analysed using RNA-seq data. Abnormal mitochondria in salivary gland epithelial cells may act as DAMPs to trigger the formation of the local immune microenvironment (23). Patients with pSS had a higher positive rate of the ANA, anti-Ro52 and anti-SSB and higher levels of serum IgG.

pSS is one of the most prevalent systemic autoimmune diseases that is characterised by a triad of manifestations: dryness, pain and

fatigue (44). Hydroxychloroquine, a common immunosuppressant, did not improve symptoms during 24 weeks of treatment of pSS (45). More clinical studies are needed to support the efficacy and safety of targeted T-cell drugs, such as Abatacept (46). Targeted B-cell agents, such as anti-B cell activating factor (BAFF) Belimumab (47) and Ianalumab (48), anti-CD20 Rituximab (47, 49), can relieve some systemic symptoms and remain the most promising therapeutic drugs for pSS (44). Therefore, new therapeutic targets targeting immune cells and the mechanisms underlying the development of pSS warrant further investigation. Mesenchymal stem cells (MSCs) treatment may provide a new therapy for pSS, since MSC treatment directed T cells toward Treg and Th2 and suppressed Th17 and Tfh responses (50).

The salivary gland epithelium is composed of acinar cells, ductal cells, MECs and progenitor cells. We have previously demonstrated that serous and mucous acini appear atrophied and the mucus content in LSGs is decreased in pSS, which may be some of the reasons for dryness in the mouth (23, 25). Salivary epithelial cells play a central role in regulating autoimmune responses by expressing various immune molecules, including human leukocyte antigen (HLA) class I molecules, CD40 (a key molecule in antigen presentation), FAS receptor (apoptosis-related molecule) and proinflammatory cytokines and chemokines (8). When salivary gland epithelial cells undergo apoptosis, the release of proinflammatory factors and ROS can induce the aggregation of

innate immune cells. These innate immune cells are recruited to the injured LSG epithelial tissue, and the activity of respiratory chain complexes and anti-apoptosis function are enhanced to exert immune effects. Mitochondria in salivary glandular epithelial cells show an abnormal structure with increased lymphocyte infiltration. A few studies have focused on the role of mitochondrial metabolites (21), such as cytochrome c (51), mtDNA (52) or ROS, in the immune microenvironment after salivary gland epithelial injury in pSS. In this study, TEM revealed mitochondrial swelling and autophagosome accumulation in scattered lymphocytes and ductal cells of the LSGs of patients with pSS, which is an important finding. Numerous studies (15, 53, 54) have shown that the swollen state of mitochondria is related to the abnormal ion channels on the mitochondrial membrane, mainly calcium channels, and the dysregulation of ROS. Correlation analysis showed that metabolic pathways related to mitochondrial swelling, such as calcium homeostasis, ROS and glutathione metabolism, did not show correlation with immune cells. Therefore, we speculate that abnormal mitochondrial function in glandular tissue leads to apoptosis and induces immune cell aggregation. Although most lymphocytes continue to function normally in pSS, damaged mitochondria in immune cells may recruit more immune cells to infiltrate, causing progressive destruction of the LSG.

Glycolysis and oxidative phosphorylation are primary sources of cellular energy. Increased oxidative phosphorylation activity often indicates cell activation and a change in function. In this study, respiratory chain complexes and oxidative phosphorylation were identified as the link between innate immune cell populations and mitochondria. Innate immune cells exhibited strong oxidative respiratory activity. Respiratory chain complexes are extremely important for the differentiation of immune cells. Blocking complex I or III can inhibit the differentiation of naïve CD4⁺ T cells into effector CD4⁺ T cells (55). Complex II is critical for oxidative phosphorylation and the TCA cycle. Defects in complex II can sensitise intestinal epithelial cells to T-cell-mediated cytotoxicity, which further induces T-cell-mediated diseases (56).

Many innate immune cells, such as monocytes and M1 macrophages, produce ATP through glycolysis instead of the TCA cycle (13). M2 macrophages mainly rely on oxidative phosphorylation to perform their immune function, whereas M1 macrophages rely on glycolysis (14). In this study, both types of cells eventually exhibited higher levels of oxidative phosphorylation. M2 macrophages were less distributed in the LSGs that were dominated by M1 macrophages in patients with pSS. These results are consistent with those of IHC analysis. In a study, single-cell RNA sequencing revealed that the expression of genes in the oxidative phosphorylation module was high in mitotic GC B cells (57). Another study reported that Treg cells impaired mitochondrial oxidative phosphorylation during an autoimmune process (17). In this study, the abundance of immune cells was not strongly associated with the expression of TCA-related genes but was strongly positively correlated with the activity of the respiratory chain complex. This finding indicates that activation of these immune cells does not rely on the TCA cycle for energy. Furthermore, ROS metabolism was positively correlated with the abundance of immune cells. Mitochondrial ROS play an

important role in intracellular signal transduction and immune regulation; however, excessive ROS production may damage cells and lead to immune regulation disorders (58). For example, a reduction in ROS levels can significantly decrease the antigen-presenting ability of pDCs (59). Therefore, alterations in oxidative phosphorylation and ROS-related signalling pathways are important features of immune cells in patients with pSS. The mitochondrial metabolic function of immune cells in the local immune microenvironment changes to exert effects on the immune response. Abnormal metabolic profiles can further recruit more immune cells, resulting in a vicious cycle. Therefore, maintaining mitochondrial function and intervening with metabolism may serve as promising strategies for the treatment of pSS in the future.

Peroxisome proliferator-activated receptor- γ (PPAR γ) coactivator 1 α (PGC-1 α) is the main regulatory component of mitochondrial biogenesis and energetic adaptation (60). PGC-1 α is an important mitochondria-related protein for the executive function of immune cells. The differentiation of human monocytes into DCs is accompanied by increased expression of PGC-1 α (16). The expression of PGC-1 α can support the formation of CD8⁺ T central memory (Tcm) cells to maintain metabolic stability and exert immune effects (61). However, in this study, the abundance of immune cells was negatively correlated with the expression of the PPARGC1A gene. We hypothesise that mitochondrial biogenesis is disrupted in dominant glandular tissue cells owing to immune cell infiltration, resulting in decreased expression of PPARGC1A. The potential role of PGC-1 α in pSS warrants further investigation.

Several reviews have summarised the relationship between immune cells and mitochondria and their metabolic function in SLE (62) and ageing (63, 64). Another important finding of this study is that the activity of mitochondria-related metabolic pathways is altered in patients with pSS. Owing to the limitations of bulk RNA sequencing technology, only overall fluctuations in the glandular immune microenvironment and mitochondria-related metabolic pathways were observed. The specific metabolic characteristics of different cell groups should be examined using more advanced technology, such as single-cell RNA sequencing and spatial transcriptome sequencing. In addition, there is a certain proportion of healthy populations and patients with organ specific autoimmune diseases show anti-Ro52 positive in the current study. In order to avoid this bias, more control cases should be included in our future studies.

Conclusion

This study suggests that innate and adaptive immune cells have distinct distribution profiles in the salivary glandular tissues of patients with pSS and highlights mitochondrial metabolic pathways that may contribute to disease progression. In response to inflammation in the glandular epithelium, some immune cells with normal mitochondria infiltrate the gland, whereas others with dysfunctional swollen mitochondria may increase inflammation in the glandular microenvironment and hence recruit more immune cells, exacerbating tissue destruction.

Data availability statement

The datasets presented in this study can be found in online repositories. The names of the repository/repositories and accession number(s) can be found below: OER378348 (<https://www.biosino.org/node/run/detail/OER378348>).

Ethics statement

The studies involving human participants were reviewed and approved by the ethics committee of Ruijin Hospital, Shanghai Jiao Tong University School of Medicine. The patients/participants provided their written informed consent to participate in this study.

Author contributions

LJ and NL designed the overall research strategy. LJ and DL wrote the manuscript. LL, YW, YYang, YYe, and JH performed the experiments. YG, NZ and XF analyzed the data. All authors contributed to the article and approved the submitted version.

Funding

This work was supported by the National Natural Science Foundation of China (NSFC No. 81900975).

References

- Verstappen GM, Pringle S, Bootsma H, Kroese FGM. Epithelial-immune cell interplay in primary sjogren syndrome salivary gland pathogenesis. *Nat Rev Rheumatol* (2021) 17(6):333–48. doi: 10.1038/s41584-021-00605-2
- Mariette X, Criswell LA. Primary sjogren's syndrome. *N Engl J Med* (2018) 378(10):931–9. doi: 10.1056/NEJMc1702514
- Fisher BA, Jonsson R, Daniels T, Bombardieri M, Brown RM, Morgan P, et al. Standardisation of labial salivary gland histopathology in clinical trials in primary sjogren's syndrome. *Ann Rheum Dis* (2017) 76(7):1161–8. doi: 10.1136/annrheumdis-2016-210448
- Bautista-Vargas M, Vivas AJ, Tobón GJ. Minor salivary gland biopsy: its role in the classification and prognosis of sjogren's syndrome. *Autoimmun Rev* (2020) 19(12):5. doi: 10.1016/j.autrev.2020.102690
- Goules AV, Tzioufas AG. Lymphomagenesis in sjogren's syndrome: predictive biomarkers towards precision medicine. *Autoimmun Rev* (2019) 18(2):137–43. doi: 10.1016/j.autrev.2018.08.007
- Singh N, Cohen PL. The T cell in sjogren's syndrome: force majeure, not spectateur. *J Autoimmun* (2012) 39(3):229–33. doi: 10.1016/j.jaut.2012.05.019
- Nocturne G, Mariette X. B cells in the pathogenesis of primary sjogren syndrome. *Nat Rev Rheumatol* (2018) 14(3):133–45. doi: 10.1038/nrrheum.2018.1
- Brito-Zeron P, Baldini C, Bootsma H, Bowman SJ, Jonsson R, Mariette X, et al. Sjogren syndrome. *Nat Rev Dis Primers* (2016) 2:16047. doi: 10.1038/nrdp.2016.47
- Hillen MR, Vervens FA, Kruize AA, Van Roon JA. Dendritic cells, T-cells and epithelial cells: a crucial interplay in immunopathology of primary sjogren's syndrome. *Expert Rev Clin Immunol* (2014) 10(4):521–31. doi: 10.1586/1744666X.2014.878650
- Wahren-Herlenius M, Dorner T. Immunopathogenic mechanisms of systemic autoimmune disease. *Lancet* (2013) 382(9894):819–31. doi: 10.1016/S0140-6736(13)60954-X
- Sandoval H, Kodali S, Wang J. Regulation of b cell fate, survival, and function by mitochondria and autophagy. *Mitochondrion* (2018) 41:58–65. doi: 10.1016/j.mito.2017.11.005
- Steinert EM, Vasan K, Chandel NS. Mitochondrial metabolism regulation of T cell-mediated immunity. *Annu Rev Immunol* (2021) 39:395–416. doi: 10.1146/annurev-immunol-101819-082015
- Faas MM, de Vos P. Mitochondrial function in immune cells in health and disease. *Biochim Biophys Acta Mol Basis Dis* (2020) 1866(10):165845. doi: 10.1016/j.bbadis.2020.165845
- Ravi S, Mitchell T, Kramer P, Chacko B, Darley-Usmar VM. Mitochondria in monocytes and macrophages-implications for translational and basic research. *Int J Biochem Cell Biol* (2014) 53:202–7. doi: 10.1016/j.biocel.2014.05.019
- Akkaya M, Traba J, Roesler AS, Miozzo P, Akkaya B, Theall BP, et al. Second signals rescue b cells from activation-induced mitochondrial dysfunction and death. *Nat Immunol* (2018) 19(8):871–84. doi: 10.1038/s41590-018-0156-5
- Pearce EJ, Everts B. Dendritic cell metabolism. *Nat Rev Immunol* (2015) 15(1):18–29. doi: 10.1038/nri3771
- Alissafi T, Kalafati L, Lazari M, Filia A, Kloukina I, Manifava M, et al. Mitochondrial oxidative damage underlies regulatory T cell defects in autoimmunity. *Cell Metab* (2020) 32(4):591–604 e7. doi: 10.1016/j.cmet.2020.07.001
- Weinberg SE, Singer BD, Steinert EM, Martinez CA, Mehta MM, Martinez-Reyes I, et al. Mitochondrial complex iii is essential for suppressive function of regulatory T cells. *Nature* (2019) 565(7740):495–9. doi: 10.1038/s41586-018-0846-z
- Cai WW, Yu Y, Zong SY, Wei F. Metabolic reprogramming as a key regulator in the pathogenesis of rheumatoid arthritis. *Inflammation Res* (2020) 69(11):1087–101. doi: 10.1007/s00011-020-01391-5
- Buang N, Tapeng L, Gray V, Sardini A, Whilding C, Lightstone L, et al. Type I interferons affect the metabolic fitness of Cd8(+) T cells from patients with systemic lupus erythematosus. *Nat Commun* (2021) 12(1):1980. doi: 10.1038/s41467-021-22312-y
- Barrera MJ, Aguilera S, Castro I, Carvajal P, Jara D, Molina C, et al. Dysfunctional mitochondria as critical players in the inflammation of autoimmune diseases: potential role in sjogren's syndrome. *Autoimmun Rev* (2021) 20(8):102867. doi: 10.1016/j.autrev.2021.102867

Acknowledgments

This work was supported by the Core Facility of Basic Medical Sciences, Shanghai Jiao Tong University School of Medicine.

Conflict of interest

The authors declare that the current research was conducted in the absence of any commercial or financial relationships that could be construed as a potential conflict of interest.

Publisher's note

All claims expressed in this article are solely those of the authors and do not necessarily represent those of their affiliated organizations, or those of the publisher, the editors and the reviewers. Any product that may be evaluated in this article, or claim that may be made by its manufacturer, is not guaranteed or endorsed by the publisher.

Supplementary material

The Supplementary Material for this article can be found online at: <https://www.frontiersin.org/articles/10.3389/fimmu.2023.1156774/full#supplementary-material>

22. Banoth B CS. Mitochondria in innate immune signaling. *Transl Res* (2018) 202:52–68. doi: 10.1016/j.trsl.2018.07.014
23. Li N, Li Y, Hu J, Wu Y, Yang J, Fan H, et al. A link between mitochondrial dysfunction and the immune microenvironment of salivary glands in primary sjogren's syndrome. *Front Immunol* (2022) 13:845209. doi: 10.3389/fimmu.2022.845209
24. Shiboski CH, Shiboski SC, Seror R, Criswell LA, Labetoulle M, Lietman TM, et al. 2016 American College of Rheumatology/European league against rheumatism classification criteria for primary sjogren's syndrome: a consensus and data-driven methodology involving three international patient cohorts. *Arthritis Rheumatol* (2017) 69(1):35–45. doi: 10.1002/art.39859
25. Li N, Li L, Wu M, Li Y, Yang J, Wu Y, et al. Integrated bioinformatics and validation reveal potential biomarkers associated with progression of primary sjogren's syndrome. *Front Immunol* (2021) 12:697157. doi: 10.3389/fimmu.2021.697157
26. Szklarczyk D, Franceschini A, Wyder S, Forslund K, Heller D, Huerta-Cepas J, et al. String V10: protein-protein interaction networks, integrated over the tree of life. *Nucleic Acids Res* (2015) 43(Database issue):D447–52. doi: 10.1093/nar/gku1003
27. Yu G, Wang LG, Han Y, He QY. Clusterprofiler: an r package for comparing biological themes among gene clusters. *OMICS* (2012) 16(5):284–7. doi: 10.1089/omi.2011.0118
28. Zhou Y, Zhou B, Pache L, Chang M, Khodabakhshi AH, Tanaseichuk O, et al. Metascape provides a biologist-oriented resource for the analysis of systems-level datasets. *Nat Commun* (2019) 10(1):1523. doi: 10.1038/s41467-019-09234-6
29. Liebermeister W, Noor E, Flamholz A, Davidi D, Bernhardt J, Milo R. Visual account of protein investment in cellular functions. *Proc Natl Acad Sci U.S.A.* (2014) 111(23):8488–93. doi: 10.1073/pnas.1314810111
30. Zhang X, Lan Y, Xu J, Quan F, Zhao E, Deng C, et al. Cellmarker: a manually curated resource of cell markers in human and mouse. *Nucleic Acids Res* (2019) 47(D1):D721–D8. doi: 10.1093/nar/gky900
31. Barbie DA, Tamayo P, Boehm JS, Kim SY, Moody SE, Dunn IF, et al. Systematic rna interference reveals that oncogenic kras-driven cancers require Tbk1. *Nature* (2009) 462(7269):108–12. doi: 10.1038/nature08460
32. Gu Z, Hubschmann D. Make interactive complex heatmaps in r. *Bioinformatics* (2022) 38(5):1460–2. doi: 10.1093/bioinformatics/btab806
33. Langfelder P, Horvath S. Wgcna: an r package for weighted correlation network analysis. *BMC Bioinf* (2008) 9:559. doi: 10.1186/1471-2105-9-559
34. Grant RA, Morales-Nebreda L, Markov NS, Swaminathan S, Querrey M, Guzman ER, et al. Circuits between infected macrophages and T cells in sars-Cov-2 pneumonia. *Nature* (2021) 590(7847):635–41. doi: 10.1038/s41586-020-03148-w
35. Rath S, Sharma R, Gupta R, Ast T, Chan C, Durham TJ, et al. Mitocarta3.0: an updated mitochondrial proteome now with Sub-organelle localization and pathway annotations. *Nucleic Acids Res* (2021) 49(D1):D1541–D7. doi: 10.1093/nar/gkaa1011
36. Liu X, Liu Y, Liu Z, Lin C, Meng F, Xu L, et al. Circmyh9 drives colorectal cancer growth by regulating serine metabolism and redox homeostasis in a P53-dependent manner. *Mol Cancer* (2021) 20(1):114. doi: 10.1186/s12943-021-01412-9
37. Ghatalia P, Gordetsky J, Kuo F, Dulaimi E, Cai KQ, Devarajan K, et al. Prognostic impact of immune gene expression signature and tumor infiltrating immune cells in localized clear cell renal cell carcinoma. *J Immunother Cancer* (2019) 7(1):139. doi: 10.1186/s40425-019-0621-1
38. Song Y, Uchida H, Sharipol A, Piraino L, Mereness JA, Ingalls MH, et al. Development of a functional salivary gland tissue chip with potential for high-content drug screening. *Commun Biol* (2021) 4(1):361. doi: 10.1038/s42003-021-01876-x
39. Liang J, Cao R, Wang X, Zhang Y, Wang P, Gao H, et al. Mitochondrial Pkm2 regulates oxidative stress-induced apoptosis by stabilizing Bcl2. *Cell Res* (2017) 27(3):329–51. doi: 10.1038/cr.2016.159
40. Hermiston ML, Xu Z, Weiss A. Cd45: a critical regulator of signaling thresholds in immune cells. *Annu Rev Immunol* (2003) 21:107–37. doi: 10.1146/annurev.immunol.21.120601.140946
41. Ganta VC, Choi MH, Kutateladze A, Fox TE, Farber CR, Annex BH. A Microrna93-interferon regulatory factor-9-Immunoresponse gene-1-Itaconic acid pathway modulates M2-like macrophage polarization to revascularize ischemic muscle. *Circulation* (2017) 135(24):2403–25. doi: 10.1161/CIRCULATIONAHA.116.025490
42. Holmes TD, Pandey RV, Helm EY, Schlums H, Han H, Campbell TM, et al. The transcription factor Bcl11b promotes both canonical and adaptive nk cell differentiation. *Sci Immunol* (2021) 6(57):2. doi: 10.1126/sciimmunol.abc9801
43. Espindola MS, Habel DM, Coelho AL, Stripp B, Parks WC, Oldham J, et al. Differential responses to targeting matrix metalloproteinase 9 in idiopathic pulmonary fibrosis. *Am J Respir Crit Care Med* (2021) 203(4):458–70. doi: 10.1164/rccm.201910-1977OC
44. Seror R, Nocturne G, Mariette X. Current and future therapies for primary sjogren syndrome. *Nat Rev Rheumatol* (2021) 17(8):475–86. doi: 10.1038/s41584-021-00634-x
45. Gottenberg JE, Ravaut P, Puechal X, Le Guern V, Sibilia J, Goeb V, et al. Effects of hydroxychloroquine on symptomatic improvement in primary sjogren syndrome: the joquer randomized clinical trial. *JAMA* (2014) 312(3):249–58. doi: 10.1001/jama.2014.7682
46. van Nimwegen JF, Mossel E, van Zuiden GS, Wijnsma RF, Delli K, Stel AJ, et al. Abatacept treatment for patients with early active primary sjogren's syndrome: a single-centre, randomised, double-blind, placebo-controlled, phase 3 trial (Asap-iii study). *Lancet Rheumatol* (2020) 2(3):e153–e63. doi: 10.1016/s2665-9913(19)30160-2
47. Mariette X, Barone F, Baldini C, Bootsma H, Clark KL, De Vita S, et al. A randomized, phase ii study of sequential belimumab and rituximab in primary sjogren's syndrome. *JCI Insight* (2022) 7(23):6–7. doi: 10.1172/jci.insight.163030
48. Bowman SJ, Fox R, Dorner T, Mariette X, Papis A, Grader-Beck T, et al. Safety and efficacy of subcutaneous ivalumab (Vay736) in patients with primary sjogren's syndrome: a randomised, double-blind, placebo-controlled, phase 2b dose-finding trial. *Lancet* (2022) 399(10320):161–71. doi: 10.1016/S0140-6736(21)02251-0
49. Bowman SJ, Everett CC, O'Dwyer JL, Emery P, Pitzalis C, Ng WF, et al. Randomized controlled trial of rituximab and cost-effectiveness analysis in treating fatigue and oral dryness in primary sjogren's syndrome. *Arthritis Rheumatol* (2017) 69(7):1440–50. doi: 10.1002/art.40093
50. Xu J, Wang D, Liu D, Fan Z, Zhang H, Liu O, et al. Allogeneic mesenchymal stem cell treatment alleviates experimental and clinical sjogren syndrome. *Blood* (2012) 120(15):3142–51. doi: 10.1182/blood-2011-11-391144
51. Kang Y SY, Zhang Y, Wang Z. Cytochrome c is important in apoptosis of labial glands in primary sjogren's syndrome. *Mol Med Rep* (2018) 17(1):1993–7. doi: 10.3892/mmr.2017.8083
52. De Benedittis G, Latini A, Colafrancesco S, Priori R, Perricone C, Novelli L, et al. Alteration of mitochondrial DNA copy number and increased expression levels of mitochondrial dynamics-related genes in sjogren's syndrome. *Biomedicine* (2022) 10(11):3–5. doi: 10.3390/biomed10112699
53. Zhou Y, Long Q, Wu H, Li W, Qi J, Wu Y, et al. Topology-dependent, bifurcated mitochondrial quality control under starvation. *Autophagy* (2020) 16(3):562–74. doi: 10.1080/15548627.2019.1634944
54. Hutto RA, Bisbach CM, Abbas F, Brock DC, Cleghorn WM, Parker ED, et al. Increasing Ca(2+) in photoreceptor mitochondria alters metabolites, accelerates photoresponse recovery, and reveals adaptations to mitochondrial stress. *Cell Death Differ* (2020) 27(3):1067–85. doi: 10.1038/s41418-019-0398-2
55. Almeida L, Dhillion-LaBrooy A, Carriche G, Berod L, Sparwasser T. Cd4(+) T-cell differentiation and function: unifying glycolysis, fatty acid oxidation, polyamines nad mitochondrial function. *J Allergy Clin Immunol* (2021) 148(1):16–32. doi: 10.1016/j.jaci.2021.03.033
56. Fujiwara H, Seike K, Brooks MD, Mathew AV, Kovalenko I, Pal A, et al. Mitochondrial complex ii in intestinal epithelial cells regulates T cell-mediated immunopathology. *Nat Immunol* (2021) 22(11):1440–51. doi: 10.1038/s41590-021-01048-3
57. Chen D, Wang Y, Manakkat Vijay GK, Fu S, Nash CW, Xu D, et al. Coupled analysis of transcriptome and bcr mutations reveals role of oxphos in affinity maturation. *Nat Immunol* (2021) 22(7):904–13. doi: 10.1038/s41590-021-00936-y
58. Kaufmann U, Kahlfuss S, Yang J, Ivanova E, Korolov SB, Feske S. Calcium signaling controls pathogenic Th17 cell-mediated inflammation by regulating mitochondrial function. *Cell Metab* (2019) 29(5):1104–18 e6. doi: 10.1016/j.cmet.2019.01.019
59. Oberkamp M, Guillerey C, Mouries J, Rosenbaum P, Fayolle C, Bobard A, et al. Mitochondrial reactive oxygen species regulate the induction of Cd8(+) T cells by plasmacytoid dendritic cells. *Nat Commun* (2018) 9(1):2241. doi: 10.1038/s41467-018-04686-8
60. Bennett CF, Latorre-Muro P, Puigserver P. Mechanisms of mitochondrial respiratory adaptation. *Nat Rev Mol Cell Biol* (2022) 23(12):817–35. doi: 10.1038/s41580-022-00506-6
61. Dumauthioz N, Tschumi B, Wenes M, Marti B, Wang H, Franco F, et al. Enforced pgc-1alpha expression promotes Cd8 T cell fitness, memory formation and antitumor immunity. *Cell Mol Immunol* (2021) 18(7):1761–71. doi: 10.1038/s41423-020-0365-3
62. Robinson GA, Wilkinson MGL, Wincup C. The role of immunometabolism in the pathogenesis of systemic lupus erythematosus. *Front Immunol* (2021) 12:806560. doi: 10.3389/fimmu.2021.806560
63. Su YJ, Wang PW, Weng SW. The role of mitochondria in immune-Cell-Mediated tissue regeneration and ageing. *Int J Mol Sci* (2021) 22(5):5. doi: 10.3390/ijms22052668
64. Han S, Georgiev P, Ringel AE, Sharpe AH, Haigis MC. Age-associated remodeling of T cell immunity and metabolism. *Cell Metab* (2023) 35(1):36–55. doi: 10.1016/j.cmet.2022.11.005